Monte Carlo simulations applied to $Al_xGa_yIn_{1-x-y}X$ quaternary alloys (X=As,P,N): A comparative study

M. Marques,[1] L. G. Ferreira,[2] L. K. Teles,[1] and L. M. R. Scolfaro[1,*]
[1]*Instituto de Física, Universidade de São Paulo, Caixa Postal 66318, 05315-970 São Paulo, São Paulo, Brazil*
[2]*Instituto de Física Gleb Wataghin, Universidade Estadual de Campinas, Caixa Postal 6165, 13083-970 Campinas, São Paulo, Brazil*
(Received 18 October 2004; published 13 May 2005)

We develop a different Monte Carlo approach applied to the $A_xB_yC_{1-x-y}D$ quaternary alloys. Combined with first-principles total-energy calculations, the thermodynamic properties of the (Al,Ga,In)X (X=As, P, or N) systems are obtained and a comparative study is developed in order to understand the roles of As, P, and N atoms as the anion X in the system $Al_xGa_yIn_{1-x-y}X$. Also, we study the thermodynamics of specific compositions in which AlGaInN, AlGaInP, and AlGaInAs are lattice matched, respectively, to the GaN, GaAs, and InP substrates. We verify that the tendency for phase separation is always towards the formation of an In-rich phase. For arsenides and phosphides this occurs in general for lower temperatures than for their usual growth temperatures. This makes these alloys very stable against phase separation. However, for nitrides the In and/or Al concentrations have to be limited in order to avoid the formation of In-rich clusters and, even for low concentrations of In and/or Al, we observe a tendency of composition fluctuations towards the clustering of the ternary GaInN. We suggest that this latter behavior can explain the formation of the InGaN-like nanoclusters recently observed in the AlGaInN quaternary alloys.

DOI: 10.1103/PhysRevB.71.205204 PACS number(s): 61.66.Dk, 64.75.+g, 71.20.Nr, 71.22.+i

I. INTRODUCTION

In the development of heterostructure-based devices, the double requirement of high-quality crystalline layers epitaxially grown on a given substrate with low-misfit-dislocation density and an optimized electronic structure are generally very difficult to achieve using the common binary and ternary compounds. Quaternary semiconducting alloys of the $A_xB_yC_{1-x-y}D$ kind are very interesting materials, because their use can be considered as an effective approach to reduce defect density in the heterostructures. Such systems allow the independent control of both lattice parameter and band-gap energy (through x and y), avoiding the lattice mismatching and, at the same time, providing an adjustable energy gap for barriers and active layers. In this sense, the lattice-matched systems such as, e.g., AlGaInAs/InP and AlGaInP/GaAs, have been extensively studied from the experimental point of view. More recently, the AlGaInN/GaN system has been studied, showing aspects not observed before. In spite of the great number of experimental works on the quaternary semiconductor alloys, there are only a few theoretical studies,[1] mainly due to the complex treatment of these systems in a more rigorous way. Particularly, the theoretical works that involve quaternary alloys make use of very simplified models, because the more rigorous treatments, such as first principles and Monte Carlo thermodynamics, are very difficult to apply. Therefore, it is highly desirable to have a method which gives very rigorous results together with a reasonable computational effort. In the present work, we develop a different Monte Carlo approach, to be used together with first-principles, self-consistent, total-energy calculations for the study of quaternary alloys. We apply this approach to study the phase-separation process of the series of III-V face-centered-cubic (fcc) pseudoternary semiconductor alloys $Al_xGa_yIn_{1-x-y}As$, $Al_xGa_yIn_{1-x-y}P$, and $Al_xGa_yIn_{1-x-y}N$, in which a microscopic description of the phase separation is performed. We make a comparative study and an individual study of each alloy for the lattice-matched systems of experimental importance.

The motivation for the study of the $Al_xGa_yIn_{1-x-y}As/InP$ lattice-matched system arises from its importance for device applications relevant to optical communications such as emitters, waveguides, lasers, and infrared detectors.[2,3] This is mainly because the band-gap energy range covered by lattice-matched quaternary alloys overlaps the region of minimum loss and dispersion current (0.8–1.2 eV) for optical fibers. The lattice-matched condition with an InP substrate is $(Ga_{0.47}In_{0.53}As)_z(Al_{0.48}In_{0.52}As)_{1-z}$, with z from 0 to 1, providing a direct energy-gap variation from 0.74 to 1.45 eV. However, a shorter lasing wavelength is required for high-density optical information processing systems. Despite the fact that AlP and GaP binary compounds present an indirect energy gaps, the phosphide ternaries and quaternaries may have higher direct energy gaps than the arsenides. Particularly, the $(Al_xGa_{1-x})_{0.5}In_{0.5}P$ quaternary alloy is lattice matched to GaAs and, except for the nitrides, it has the largest direct energy gap among the III-V semiconductors, with the emission wavelength being tunable from red to green by changing the amount of Al. For laser diodes, the AlGaInP forms the barrier with the active layer being the GaInP ternary compound or even the quaternary compound with a lower Al concentration. The main commercial interest in devices based on these systems is in the continuing evolution of compact-disk technology (now based on the AlGaAs/GaAs system, providing a 780-nm emission) towards the digital-video-disk (DVD) technology. The current generation of DVD's uses an AlGaInP red laser with an emission wavelength of 650 nm. Shorter wavelengths (higher band gaps), though desirable, lead to poor AlGaInP-sample quality and an indirect band gap. These two factors imply a very-low-emission efficiency.

Bulk AlGaInP, like AlGaInAs, is very stable against clustering or phase separation. In the whole compositional range of the quaternary lattice matched to GaAs, a good structural quality and high compositional uniformity is obtained.[4] However, there are surface effects that lead to different phases rather than solid solution. Through the combined effects of the surface thermodynamics and kinetics, the composition modulation and the CuPt-ordered structure can exist together in the AlGaInP matrix.[5] The ordering dramatically affects the electronic properties of the material, and in particular reduces the direct-energy-gap. Therefore, this phase is undesirable for device applications as it leads to longer wavelength emission, and, because the ordering is not uniform, the resulting large-crystal inhomogeneity likely leads to inferior device performance. But the generation of ordered structures can be suppressed by several means, such as the increase of the growth temperature[6] above 700 °C, the use of misoriented substrates, and the use of *p*-type doping.[7]

In the last few years, great progress has been made in the research of GaN and related semiconductors, which present larger energy gaps than the phosphides and arsenides. As a result, blue-green light-emission diodes (LEDs) as well as ultraviolet (UV) laser diodes (LDs) have been commercialized.[8] Recently, the AlGaInN quaternary alloys attracted much attention due to the fact that lattice-matched materials can be obtained with a possible energy gap in the deep-UV region. In addition, the incorporation of Indium in the AlGaN ternary alloy, forming the AlGaInN quaternary alloy has now been demonstrated to improve the optical quality of the alloy layer for the UV-emission alloy,[9] even when the Al content is increased. Until now it had not been possible to grow good-quality material in the whole compositional range, and the majority of the samples presents an In concentration lower than 4%. But, despite these problems, an increasing number of experimental works on AlGaInN have been presented. The successful applications are the recently produced nearly lattice-matched AlGaInN/GaInN UV LDs,[10] the AlGaInN/AlGaInN deep-UV LEDs, and the UV LDs.[11,12] These optical devices can emit a wavelength smaller than 400 nm, which is a great improvement in our capacity for information storage. Nevertheless, questions concerning this complex system remain still open. For example, the emission mechanism involved in the UV spectra is frequently associated to the existence of In-rich phases or GaInN-like clusters, and not to the band-to-band transition in the quaternary alloy itself.[13,14] Moreover, some samples show a green emission around 2.4 eV besides the UV emission.[15] These facts lead to the possibility of a phase-separation process in this alloy. Several works show evidence of alloy inhomogeneities, with the formation of possible clusters in the matrix of the alloy.[13,14] But the questions of how the In nucleation takes place in the bulk of the AlGaInN quaternary alloys (in which components the alloy separates) and what the relation is between the In-separated phases remain under discussion.

Therefore, we not only develop an approach for the study of $A_xB_yC_{1-x-y}D$ quaternary systems, but also present a rigorous and systematic theoretical study of the thermodynamic properties of some important quaternary systems, from which we can obtain new features of their phase-separation processes. The paper is organized as follows. In Sec. II we describe the details of the calculation methods. In Sec. III we discuss alloy stabilities and analyze the experimentally relevant lattice-matched systems. Finally, a summary is given in Sec. IV.

II. CALCULATION METHODS

In this section we describe the main ideas behind the computational methods used in this paper.

A. The ternary expansion and the Monte Carlo approach

In a ternary alloy $A_xB_yC_{1-x-y}$ or pseudoternary (quaternary) alloy $A_xB_yC_{1-x-y}D$, the sites of a crystal lattice are occupied by *A*, *B*, and *C* atoms in different configurations. To perform Monte Carlo studies one requires, in principle, a sampling of the 3^N possible configurations of *A*, *B*, and *C* atoms in *N* lattice sites, where *N* is about 10^4. This is a formidable task for first-principles electronic-structure methods, as it involves a huge number of calculations. To circumvent this problem it is necessary to describe any arrangement of *N* atoms in terms of a few arrangements of a much smaller number of atoms. The classical way to accomplish this description is by means of a cluster expansion. In the case of binary (A_xB_{1-x}) or pseudobinary ($A_xB_{1-x}C$) alloys, cluster expansions have reached a high degree of sophistication.[16–18] In the case of quaternary alloys, though the theory is well developed,[19] cluster expansions are not as useful, because they are not as simple.

In this paper, instead of cluster expansions we develop a different approach. In particular, we study $A_xB_yC_{1-x-y}D$ alloys that crystallize in the zinc-blende structure, where the atoms *A*, *B*, and *C* occupy one fcc sublattice, and the atoms *D* the other fcc sublattice, although the basic idea of the method can be applied for other kinds of structures. We assume an unstrained alloy, which means that there is no constraint on the lattice parameter and the alloy is allowed to have its own lattice constant. In our approach, we consider all arrangements of atoms *A*, *B*, and *C* in an enlarged periodic fcc lattice with repeating unit vectors (0*aa*), (*a*0*a*), and (*aa*0). These are twice the primitive vectors

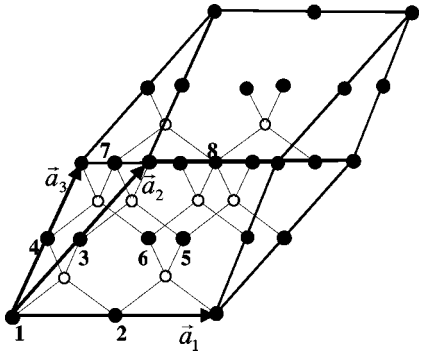

FIG. 1. The hexahedron unit cell (stretched cube along a body diagonal) with the respective eight cation sites. $\vec{a}_1$, $\vec{a}_2$, and $\vec{a}_3$ are the primitive vectors.

TABLE I. Four possible choices for the basis of the eight-atom cell (hexahedron). The lattice parameter is set to $a=2$. Sites in the same column are related by translation vector combinations of (022), (202), or (220). The last line in the table is used to produce the ternary number.

	Sites in the eight-atom cell							
Possible basis	Site 1	Site 2	Site 3	Site 4	Site 5	Site 6	Site 7	Site 8
1	(0,0,0)	(0,1,1)	(1,0,1)	(1,1,0)	(2,1,1)	(1,2,1)	(1,1,2)	(2,2,2)
2	(0,0,0)	(0,−1,−1)	(1,−2,−1)	(1,−1,−2)	(2,−1,−1)	(1,0,−1)	(1,−1,0)	(2,−2,−2)
3	(0,0,0)	(−2,1,−1)	(−1,0,−1)	(−1,1,−2)	(0,1,−1)	(−1,2,−1)	(−1,1,0)	(−2,2,−2)
4	(0,0,0)	(−2,−1,1)	(−1,−2,1)	(−1,−1,0)	(0,−1,1)	(−1,0,1)	(−1,−1,2)	(−2,−2,2)
	3^7	3^6	3^5	3^4	3^3	3^2	3^1	3^0

$(0,a/2,a/2)$, $(a/2,0,a/2)$, and $(a/2,a/2,0)$, of the fcc lattice so that the larger unit cell contains eight original fcc sites. The unit cell, which is a hexahedron (stretched cube along a body diagonal), and the eight cation sites are schematically shown in Fig. 1. The number of possible arrangements of atoms in the enlarged unit cell is $3^8=6561$. Most arrangements are related by the rotation-inversion translations of the zinc-blende space group. Grouping the symmetry-related arrangements we obtain 141 *classes*.[20] This will be the number of first-principle energy calculations used to describe all the arrangements (configurations) of the system.

The eight-site unit cell can be chosen from any of the four listed in Table I and pictured in Fig. 2. The sites of the four hexahedra are related by the enlarged fcc translations with unit vectors $(0aa)$, $(a0a)$, and $(aa0)$. The extreme sites of the four hexahedra are a tetrahedron with vertices at (aaa), $(\bar{a}aa)$, $(\bar{a}\bar{a}a)$, $(a\bar{a}a)$. (In the case of Table I and Fig. 2 we set $a=2$.) The many arrangements of atoms in a hexahedron can be represented by *ternary* numbers, which unequivocally identify the arrangement. In order to have a ternary number, first we call the *A*, *B*, and *C* atoms 0, 1, and 2, respectively. Consider, for example, a possible configuration, where the eight sites of our unit cell are occupied by the atoms *C*, *A*, *B*, *C*, *C*, *B*, *A*, and *B*; in our new notation they correspond to 2, 0, 1, 2, 2, 1, 0, and 1, respectively. Each site of the unit cell corresponds to a number with a basis of 3 and an exponent *n* from 0 to 7 in such a way that the site 1,2,3,…,8 corresponds to $3^7,3^6,3^5,\ldots,3^0$. Therefore, the example configuration is represented by the ternary number $2\times3^7+0\times3^6+1\times3^5+2\times3^4+2\times3^3+1\times3^2+0\times3^1+1\times3^0=20122101_3=4843$. Thus, there are only 141 ternary numbers corresponding to arrangements not related by symmetry.

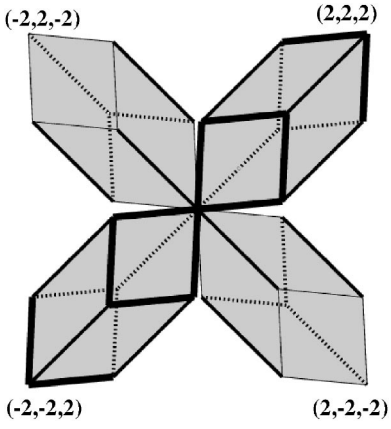

FIG. 2. (001) projection of the four hexahedra associated with a site. The hexahedra are slightly deformed for a better visualization. They are oriented along the body diagonals forming a tetrahedron. The very thick lines are ascending in the (001) direction. The thin full lines are descending. The intermediate thick lines stay perpendicular to (001). The dotted lines are behind the higher faces of each hexahedron.

Table II lists the configurations of atoms 0, 1, and 2 in a cell of *N* sites, having the largest space groups. The configurations are ordered by the size of their space groups (size of the zinc-blende space group/size of the configuration space group). Many *N*-site configurations are special arrangements of atoms in the hexahedral cell. These are indicated in the table by the corresponding ternary number in the last column. Many configurations are superlattices, as indicated in the second column of the table. In the third column of the table we indicate the name of the configuration, when it is known. For those *N*-site configurations that are not arrangements in the eight-site hexahedral cell, we indicate their linear combinations of ternary number arrangements in the last column of Table II. In what follows we explain how to find these linear combinations.

We define the energy of any configuration of atoms in the *N* sites of a Monte Carlo cell as follows. First, the first-principle total energies for the 141 classes are calculated. In our case we adopt a first-principles pseudopotential plane-wave code within density functional theory and the local density approximation (DFT LDA), the "Vienna *Ab Initio* Simulation Package" (VASP)—details will be given in Sec. II B.[21] Since for each ternary *T* in the range $0\leqslant T\leqslant3^8-1$ we know to which class it belongs, the first-principle calculations lead to the knowledge of the energy function $e(T)$ of a ternary. Next, assume that the total energy of the Monte Carlo cell is a sum of the site energies, which in turn is an average of the energies of the four hexahedra listed in Table I and pictured in Fig. 2. In other words, given the configuration of atoms in the Monte Carlo cell, we know the ternary for each of the four hexahedra with origins at each site. Let $T(n,i)$ with $1\leqslant n\leqslant N$ and $1\leqslant i\leqslant4$ be the ternary for the *i*th hexahedron centered at the site *n*. Then the total Monte Carlo cell energy is written as

TABLE II. Highest symmetry configurations of atoms *A*, *B*, and *C* in a zinc-blende-fcc lattice. The very highest symmetry configurations are arrangements in the hexahedral unit cell and are characterized by *ternary* numbers. Each typical ternary number is representing classes with the same symmetry, but different compositions. For instance, the ternary 10000001_3 also represents the classes 20000002_3, 12222221_3, 21111112_3, 01111110_3, and 02222220_3 ($L1_2$). Many high-symmetry configurations are superlattices with definite vectors and repeating patterns of planes. The names of the configurations, when known, follow those of Ref. 34. The configurations not corresponding to *ternary* numbers, which are not arrangements of the hexahedral cell, can be expanded in terms of the *ternaries* (see text).

Size of the zinc-blende space group / Size of the configuration space group	Superlattice	Name	Ternary number representation
1		fcc	11111111_3
4		$L1_2$	10000001_3
6	(0 0 1) [*BA*]	$L1_0$	10100101_3
8	(1 1 1) [*BA*]	$L1_1$	11100010_3
8		*D*1	10000000_3
8		*D*4	11110000_3
8			20000001_3
9	(0 0 1) [*BAA*]	$\beta 1$	$\frac{2}{3}11000000_3+\frac{1}{3}11001001_3$
12	(1 1 1) [*BAA*]	$\alpha 1$	$\frac{1}{4}00000000_3+\frac{1}{6}11100000_3$ $+\frac{1}{12}10000001_3+\frac{1}{2}11100010_3$
12	(1 1 1) [*CBA*]		$\frac{1}{4}11100010_3+\frac{1}{4}22200020_3$ $+\frac{1}{4}22211121_3+\frac{1}{12}22210010_3$ $+\frac{1}{12}00021121_3+\frac{1}{12}11102202_3$
12	(0 0 1) [*BAAA*]	*Z*1	$\frac{1}{4}00000000_3+\frac{1}{2}11000000_3$ $+\frac{1}{4}11001001_3$
12	(0 0 1) [*BBAA*]	*Z*2	$\frac{1}{2}11000000_3+\frac{1}{2}00111111_3$
12	(0 0 1) [*CABA*]		$\frac{1}{4}11001001_3+\frac{1}{4}22002002_3$ $+\frac{1}{2}22001001_3$
12			21001002_3
12	(2 1 0) [*BAAA*]	DO_{22}	$\frac{1}{2}11000000_3+\frac{1}{2}10000001_3$
12	(2 1 0) [*CABA*]		$\frac{1}{2}22001001_3+\frac{1}{2}21001002_3$
12	(2 1 0) [*BBAA*]	'40'	11100001_3

$$E=\frac{1}{4}\sum_{n=1}^{N}\sum_{i=1}^{4}e[T(n,i)]. \tag{1}$$

$$\Delta E|_l=\frac{1}{4}\sum_{\substack{n,i\\(n,i)\supset l}}e[T(n,i)']-e[T(n,i)]. \tag{2}$$

The set of 141 ternary numbers is then used in the expansion of Eq. (1) to predict the total energies for another set of periodic structures. This prediction is compared with the directly calculated values from electronic structure theory. In Table III we present the configuration energies calculated by local density approximation (LDA) and the corresponding prediction of Eq. (1), for some nitride quaternary alloys. The maximum error of 0.03 eV/cation is very small for our purposes.

To make Monte Carlo runs we compute the excitation energy when the atom of a site l is changed. Assume that the hexahedron (n,i) (ith hexahedron of site n) contains the site l whose atom has been changed $[(n,i)\supset l]$. Compute the new ternary number $T(n,i)'$. The excitation energy is then given by

There are $4\times 8=32$ hexahedra containing a given site whose atom is changed.

We used the standard Metropolis[22] algorithm in attempting to exchange atoms of neighboring sites only. In the process the concentrations x and y are kept constant. At each atom-exchange attempt between sites l and m one calculates the energy differences according to Eq. (2). Changing the atom of a site implies changing the ternary numbers of only 32 hexahedra. For comparison, if we were to use the simplest cluster expansion with the nearest-neighbor pair, triangle, and tetrahedra, changing one atom would imply recalculating the products of spins of $12+24+8=44$ figures. Therefore the present version of Monte Carlo is both fast and easily programmable.

TABLE III. Test of the expansion of Eq. (1) to predict the total energies of a set of periodic basic structures. This prediction is compared with the directly calculated values from electronic structure theory. The fourth column gives the difference per atom between the two cases.

Structure	Expansion of Eq. (1) (eV/atom)	LDA calculation (eV/atom)	Difference (meV/atom)
β1-AlGaGa	−7.4090	−7.4101	1.0170
β1-AlInIn	−6.7897	−6.7984	8.6874
β1-GaAlAl	−7.8060	−7.8065	0.5340
β1-GaInIn	−6.4048	−6.4110	6.2137
β1-InAlAl	−7.4596	−7.4764	16.8020
β1-InGaGa	−6.6797	−6.6926	12.9240
α1-AlGaGa	−7.4084	−7.4073	1.1105
α1-AlInIn	−6.7778	−6.7495	28.2460
α1-GaAlAl	−7.8052	−7.8038	1.3588
α1-GaInIn	−6.3998	−6.3836	16.2221
α1-InAlAl	−7.4524	−7.4232	29.1951
α1-InGaGa	−6.6784	−6.6613	17.1001
*Z*1-AlGaGaGa	−7.3103	−7.3100	0.3207
*Z*1-AlInInIn	−6.6355	−6.6367	1.1853
*Z*1-GaAlAlAl	−7.9055	−7.9057	0.1687
*Z*1-GaInInIn	−6.3468	−6.3479	1.0624
*Z*1-InAlAlAl	−7.6458	−7.6524	6.6274
*Z*1-InGaGaGa	−6.7633	−6.7699	6.5586
*Z*2-AlAlGaGa	−7.6071	−7.6076	4.4163
*Z*2-AlAlInIn	−7.1197	−7.1285	8.8106
*Z*2-GaGaInIn	−6.5409	−6.5474	6.5031

B. The first-principles calculations of the basic configurations

The total energy of each configuration is calculated by adopting a first-principles pseudopotential plane-wave code based on the density functional theory (DFT) in the local density approximation (LDA),[23] the Vienna *Ab initio* Simulation Package (VASP).[21] Besides the valence electrons, the semicore Ga3*d* and In4*d* states are also explicitly considered. Their interaction with the atomic cores is treated with the non-norm-conserving *ab initio* Vanderbilt pseudopotentials.[24] The many-body electron-electron interaction is described within the Ceperley-Alder scheme as parametrized by Perdew and Zunger.[25] The **k**-space integrals are approximated by sums over a $4\times4\times4$ special point of the Monkhorst-Pack type[26] within the irreducible part of the Brillouin zone. Sixteen-atom (eight cations and eight anions) supercells are used as the repeating units of the alloy configurations. Considering the symmetry, there are 141 classes of configurations that are distinguished by the distinct relaxed configuration energies ε_j. The total-energy calculations of the 141 classes are performed at $T=0$ K. The plane-wave expansion is restricted to an energy cutoff of 331.5 eV for nitrides and 313.4 eV for arsenides and phosphides. For the nitrides, the structure of each class is optimized with respect to its lattice constant, via a total-energy minimization. In the cases of arsenides and phosphides, the optimization of the lattice constant is only carried through for the binary compounds, and the lattice constant for the others clusters is obtained assuming the Vegard's law.[27] But, in all three different cases, the atomic coordinates in the supercell are relaxed by diminishing the Hellmann-Feynman forces till the energy difference between two consecutive changes of atomic positions is $\leqslant10^{-4}$ eV.

C. Studying the stability of the alloys: The affinity parameter

In order to quantify the Monte Carlo results and to analyze in more detail what is happening on a microscopic scale, i.e., how the atoms are distributed in the equilibrium, if they are randomly displayed, or if there are nucleations of a certain kind of atom, we defined a quantity named as affinity (α), which is similar to the Warren-Cowley parameter.[28] The concentration of atoms *A*, *B*, and *C* in the alloy is *x*, *y*, $(1-x-y)$, respectively, which we will call simply x_A, x_B, and x_C. In a random distribution, considering a certain atom, the number of its first cation neighbors of the kind *B* is on average 12 times x_B. The affinity represents how much the first neighborhood deviates from the one in a random distribution. In other words, by considering the equilibrium Monte Carlo (MC) cell, analyzing the number of first cation neighbors of each atom, and comparing it with the number in the case of a random alloy, we can make conclusion about the tendency of individual components to stay close or far away from each other. Therefore, the affinity between atoms *A* and *B* is defined as

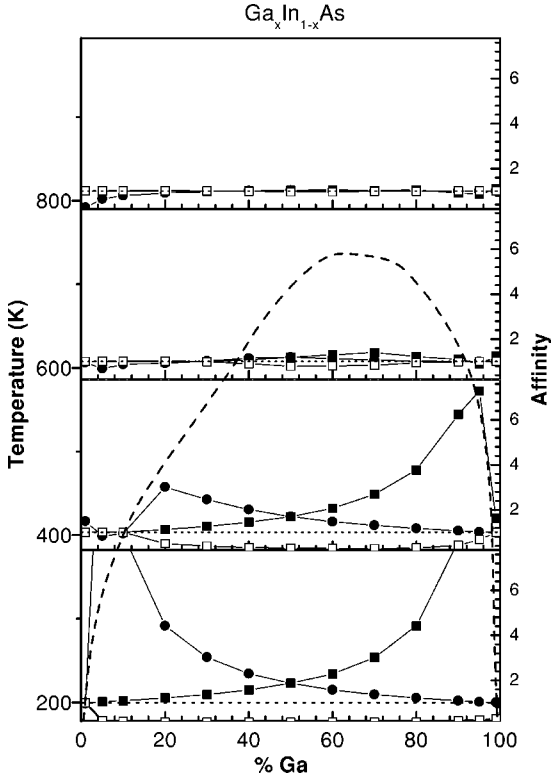

FIG. 3. Description, in terms of the affinities, of the distribution of atoms in the thermodynamically stable Monte Carlo cell in the test case of the $Ga_xIn_{1-x}As$ ternary alloy. The calculation was performed for temperatures of 200, 400, 600, and 800 K. The dashed line indicates a schematic binodal line corresponding to the Monte Carlo results. The affinities are represented by full circles (Ga-Ga), full squares (In-In), and empty squares (Ga-In).

$$\alpha_{A-B} = \frac{\overline{n}_{A-B}}{12x_B}, \tag{3}$$

where $\overline{n}_{A-B}$ is, considering an atom A, the average number of the first neighbors of kind B in the equilibrium MC cell. Observe that the definition of the affinity comprises three interesting situations: (i) if $\alpha_{A-B} \sim 1$ the distribution is considered random; (ii) if $\alpha_{A-B} > 1$ there is a predominance of B atoms in the first neighborhood of atom A, i.e., the A and B atoms tend to attract each other; and (iii) if $\alpha_{A-B} < 1$ there is an absence of B atoms in the first neighborhood of the A atom, meaning repulsion.

III. RESULTS AND DISCUSSION

In this section we apply our approach to the series of III-V quaternary alloys, make a comparative study between them, and analyze the experimentally relevant cases.

A. Ground-state search and Monte Carlo simulations

The use of the energy expansion in the energies of the 141 classes allows us to perform a restricted ground-state search, comparing different structures of the same composition.[16] This search leads to the conclusion, for the three studied quaternaries, that the only stable compounds are the binaries. Thus the quaternaries, and even the ternaries, tend to phase separately.

Having identified the lower-energy configurations, we use MC simulations[22] to calculate the temperature and composition ranges in which the alloy is stable. The MC dynamics was made, keeping the concentrations x and y constant (canonical Monte Carlo), by exchanging neighboring atoms only. We used a MC cell of $23^3 = 12\,167$ fcc sites, which can be considered a reliable size to simulate the alloys, and 10^4 atom-exchange attempts per site. The latter value was tested, verifying that the thermodynamic-equilibrium distribution of atoms in the MC cell was reached.

B. Equilibrium, fluctuations, and phase separation

First, we analyze our method by using the prototype semiconductor $Ga_xIn_{1-x}As$. In Fig. 3 are depicted the results for the affinities between the cations, by considering four different temperatures. We consider a range of temperatures from $T = 200$ K to $T = 800$ K with ΔT equal to 200 K and evaluate the affinities for these four temperatures. We observe that for $T = 800$ K the affinities are $\simeq 1$, which means that the system should be approximately random. For $T = 600$ K, we can already observe that the affinities are different from one for a Ga concentration from 40 to 90%. This result is particularly interesting, since it shows an asymmetry of the miscibility gap, in very good agreement with previous results.[29] For $T = 400$ K and $T = 200$ K, the miscibility gap becomes greater and greater, as expected. Only to illustrate, we draw a dashed line through the onset of increasing affinity, and it clearly resembles a typical binodal curve in excellent agreement with published results.[29] It is worth pointing out that, for all ternaries, we also obtained very good results when compared with the known results already in the literature.[29–31]

Now we focus our attention on the quaternaries. Our aim is to study the stability of the $Al_xGa_yIn_{1-x-y}X$ quaternary alloys (with X=N, P, and As) and to make a comparative study between them. Then, first we consider the same set of compositions (x,y) for all three alloys and study the affinities between the atoms by varying the temperature. In particular, we choose the compositions commonly used for the nitride quaternary alloys, 4% In and 20% Al. The behavior of the affinities is depicted in Figs. 4–6, respectively, for nitrides, phosphides, and arsenides. We can observe that for the high temperature $T > 1300$ K, the three systems all present affinity values near 1, i.e., $\alpha_{X-Y} \approx 1$, which means that there is no phase separation, and the alloys are approximately random. As the temperature decreases, inhomogeneities in the distribution of atoms take place, which are represented in this description by values of affinities higher or smaller than 1. In what follows we describe in detail the behavior of each quaternary alloy.

Figure 4 presents the results for the $Al_{0.20}Ga_{0.76}In_{0.04}N$ alloy. We observe that the system is approximately random for $T > 1300$ K and that below this temperature the In-In affinity abruptly increases, accompanied by a decrease of the Al-In and Ga-In affinities. It is a remarkable fact that the Al-In affinity is even smaller than the Ga-In affinity. This

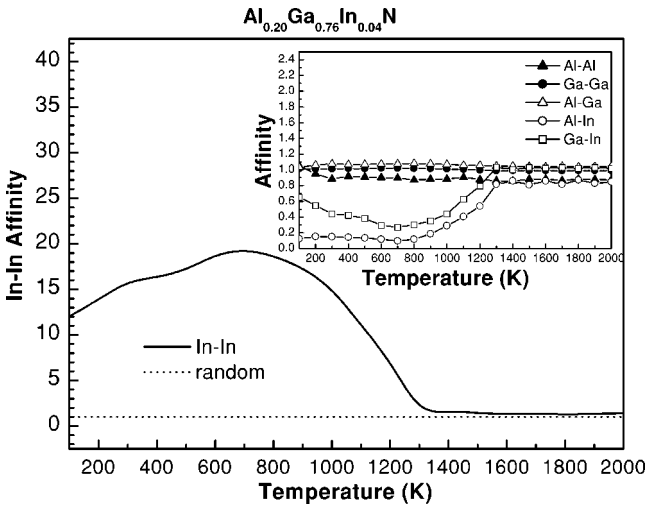

FIG. 4. In-In affinity versus temperature for the $Al_{0.20}Ga_{0.76}In_{0.04}N$ quaternary alloy. The Al-Al, Ga-Ga, Al-Ga, Al-In, and Ga-In affinities versus temperature are presented in the inset.

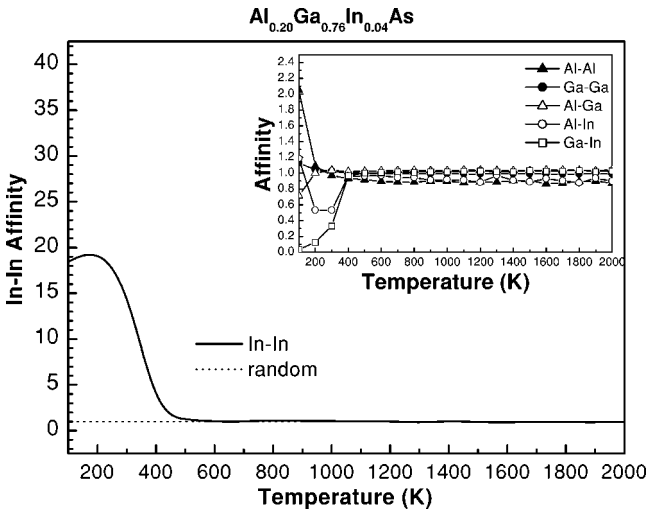

FIG. 6. In-In affinity versus temperature for the $Al_{0.20}Ga_{0.76}In_{0.04}As$ quaternary alloy. The Al-Al, Ga-Ga, Al-Ga, Al-In, and Ga-In affinities versus temperature are presented in the inset.

behavior of the affinities indicates the formation of In-rich regions, with the neighborhood of the In atoms having 20 times more In atoms than a random alloy, a small number of Ga atoms, and a negligible number of Al atoms. Therefore, there is a strong phase separation in the system. In the cases of $Al_{0.20}Ga_{0.76}In_{0.04}P$ and $Al_{0.20}Ga_{0.76}In_{0.04}As$ (Figs. 5 and 6) the same behavior is observed as in the case of the nitrides, but with two main differences: (i) the phase separation occurs just for low temperatures, approximately $T<500$ K and $T<400$ K for the $Al_{0.20}Ga_{0.76}In_{0.04}P$ and $Al_{0.20}Ga_{0.76}In_{0.04}As$ alloys, respectively; and (ii) in the regime of the phase separation, the Ga-In affinity is smaller than the Al-In affinity.

Despite the tendency of the three quaternaries towards the formation of In-rich phases, the temperatures for the transitions are very different. The arsenides and phosphides are much more stable against phase separation than the nitrides. This behavior can be understood by the lattice mismatch between the binaries that compound the respective quaternary alloys. A large lattice mismatch means that the bond lengths of the binaries are very different and, if they are forced into a unique lattice, they cause large internal strains favoring decomposition. The nitrides having the largest mismatches will be the most likely to present phase separation. In the case of the nitrides, the value of the bond length increases from Al-N to In-N passing through the Ga-N. Therefore, in the regime of phase separation, the presence of Al atoms close to the In atoms is even more unlikely than the presence of Ga ($\alpha_{\text{Al-In}}<\alpha_{\text{Ga-In}}$). This order is reversed in phosphides and arsenides because the Ga-P and Ga-As bond lengths are a little bit smaller than the Al-P and Al-As ones, respectively.

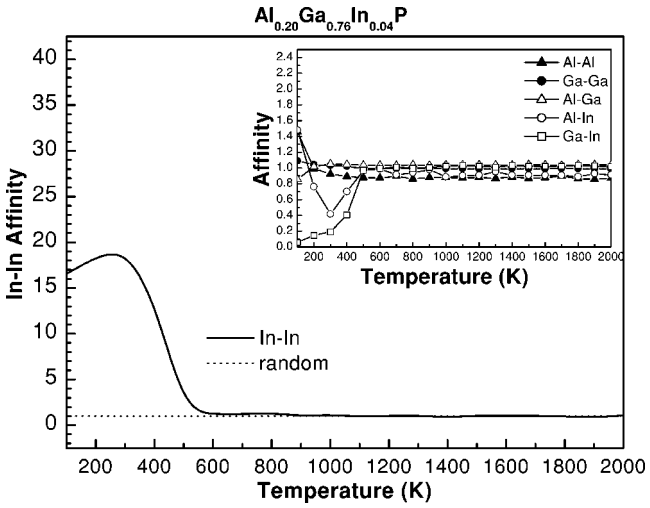

FIG. 5. In-In affinity versus temperature for the $Al_{0.20}Ga_{0.76}In_{0.04}P$ quaternary alloy. The Al-Al, Ga-Ga, Al-Ga, Al-In, and Ga-In affinities versus temperature are presented in the inset.

We also studied the thermodynamics of these quaternary alloys with different compositions: an alloy with a medium concentration of In (25% In and 25% Ga) and an alloy with high In concentration (50% In and 25% Ga). As the main signature of the separation process is the formation of In-rich phases, in Fig. 7 we present only the In-In affinity for the three systems. Some general tendencies can be observed. The increase of the In concentration increases the temperature below which phase separation occurs, leading the system to be more unstable. In particular, in the cases of $Al_{0.25}Ga_{0.25}In_{0.50}X$ and $Al_{0.50}Ga_{0.25}In_{0.25}X$, all calculated temperatures presented phase separation for the nitrides. Comparing the three systems, the phase separation always occurs at higher temperatures in nitrides than in phosphides and arsenides. In the case of the latter, the distribution of atoms deviates from random only at very low temperatures. The maximum value of the In-In affinity is of the same order of magnitude in the three alloys. We can observe that, decreasing the temperature from 2000 K, the specific temperature when phase separation occurs is higher for the nitrides, followed by the phosphides and the arsenides.

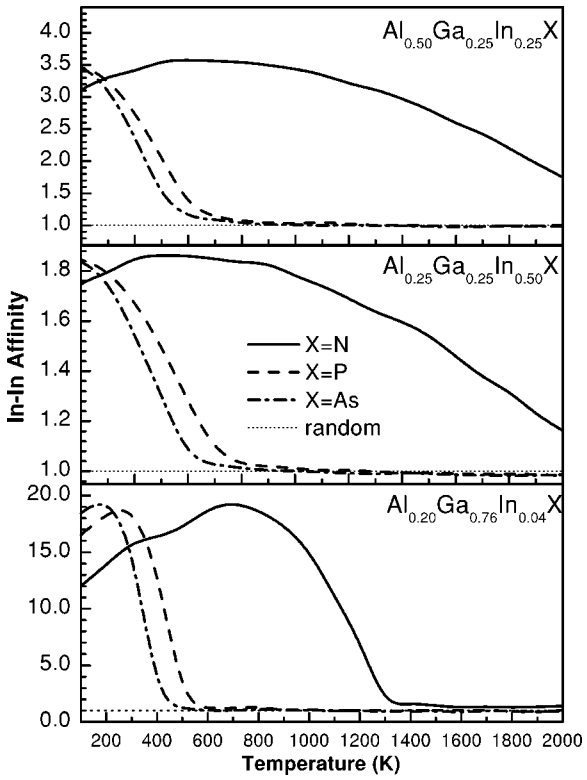

FIG. 7. Comparative study of the In-In affinity versus temperature for nitrides, phosphides, and arsenides with different compositions.

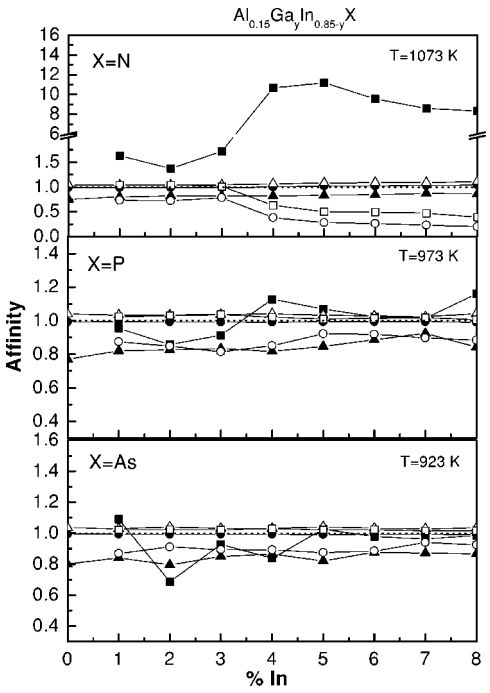

FIG. 8. Affinities as functions of the In composition for the $Al_{0.15}Ga_yIn_{0.85-y}X$ system (X=As, P, or N). The calculation is carried through for the typical growth temperature, 1073 K for AlGaInN, 973 K for AlGaInP, and 923 K for AlGaInAs. The affinities are represented by full triangles (Al-Al), full circles (Ga-Ga), full squares (In-In), empty triangles (Al-Ga), empty circles (Al-In), and empty squares (Ga-In).

Aside from the two regimes of complete randomness and clear phase separation, we also observed an intermediate regime in the case of the nitrides. In Fig. 8 we present the affinities at the quaternary growth temperatures. The figure shows an intermediate regime, peculiar to the nitrides, for In concentration $<4\%$. In this regime $\alpha_{\text{In-In}} \approx 1.5$, $\alpha_{\text{Gn-In}} \approx 1$ and $\alpha_{\text{Al-In}} \approx 0.7$, indicating a tendency towards GaInN clustering, instead of InN clustering. The InN clustering at the growth temperature happens only at higher In concentrations. On the other hand, at their growth temperatures and in the same range of compositions, AlGaInP and AlGaInAs present regimes of complete randomness (all affinities around 1).

The presence of an intermediate regime for the nitrides can be clearly observed by looking at the distribution of atoms in the MC cell in Fig. 9. There we observe the local clustering of GaInN in the MC cell with 3% In. We believe that this behavior is related to the GaInN clusters recently observed by Chen *et al.*[14] at room-temperature micro-Raman and scanning electron microscopy measurements. In the same work they also show evidence that the strong UV emission comes from this GaInN nanocluster, explaining the superior UV emission of AlGaInN compared with the ternary AlGaN whose emission is band-to-band. Also in Fig. 9, we can see that in the MC cell with 5% In, the system presents a phase separation with an In-rich phase formation. Experimentally, a phase separation process was also observed, presenting a green emission together with the UV emission.[15] Following our result, those samples would have a high In-In affinity, giving rise to In-rich clusters inside the alloy matrix. We think that this confined region would be responsible for the low-energy peak emission in addition to the UV emis-

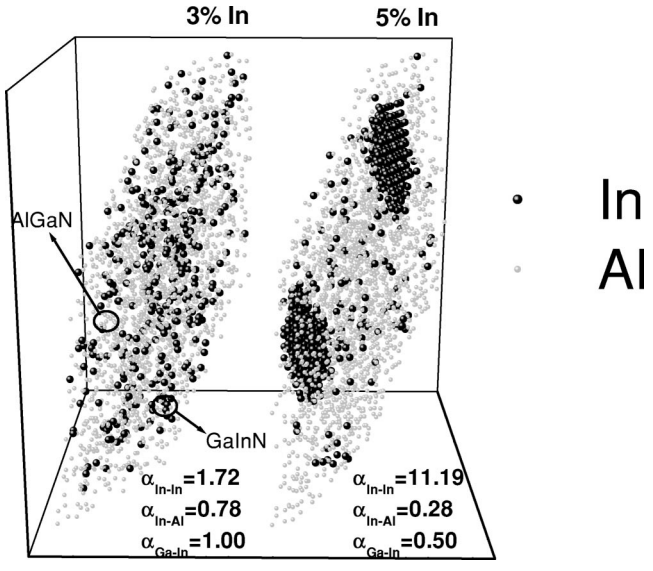

FIG. 9. Stable distribution of atoms in the Monte Carlo cell with 12 000 atoms, in the cases of GaInN clustering (3% In) and the phase separation of the InN rich phase (5% In). The temperature is 800 °C, the Al content is fixed in 20%, and only the Al and In atoms are shown.

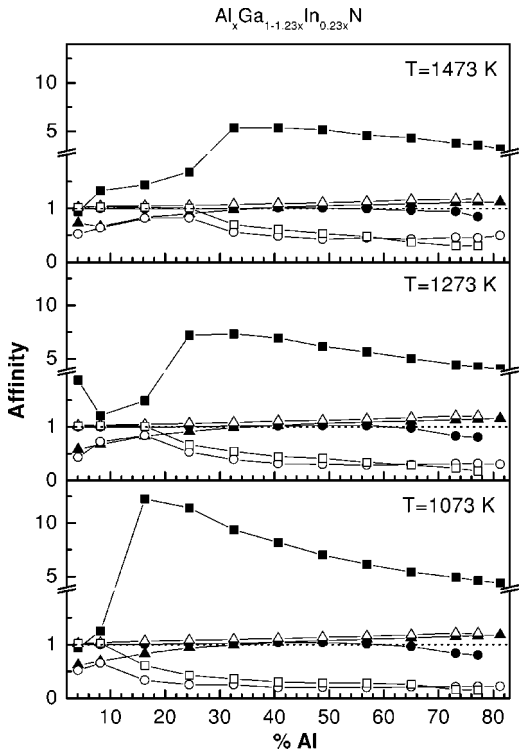

FIG. 10. Affinities versus Al concentration in the region of composition where the AlGaInN quaternary is lattice matched to GaN. The affinities are represented by full triangles (Al-Al), full circles (Ga-Ga), full squares (In-In), empty triangles (Al-Ga), empty circles (Al-In), and empty squares (Ga-In).

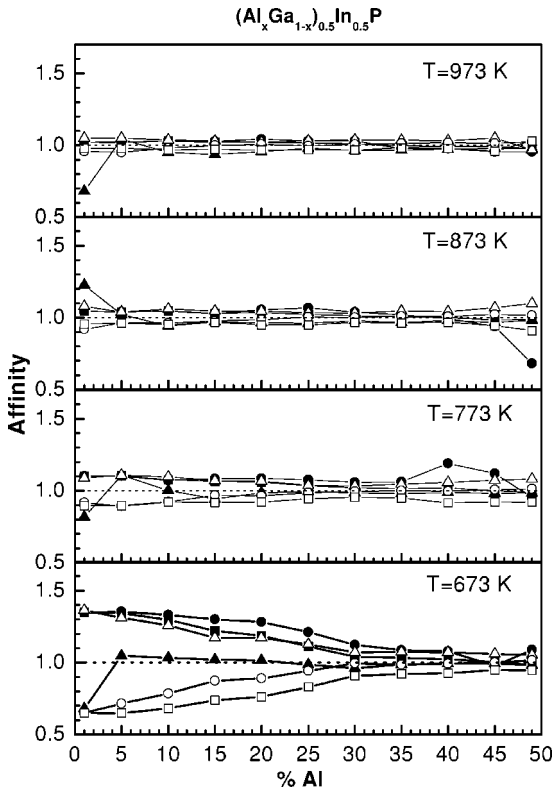

FIG. 11. Affinities versus Al concentration in the region of composition where the AlGaInP quaternary is lattice matched to GaAs. The affinities are represented by full triangles (Al-Al), full circles (Ga-Ga), full squares (In-In), empty triangles (Al-Ga), empty circles (Al-In), and empty squares (Ga-In).

sion coming from the matrix, since the InN presents a lower energy gap compared with the GaInN ternary alloy. The double emission happens in samples grown at 1073 K with low In concentrations. This model for the double emission mechanism in the AlGaInN quaternary alloy was recently proposed by us in a previous work.[32] Thus our results give an explanation for the different emission channels observed in the nitride samples.

C. Lattice-matched quaternary alloys

Figure 10 presents the case of the AlGaInN quaternary alloy lattice-matched to GaN. The usual growth temperature for this alloy is about 800 °C. As can be observed, the alloy presents phase separation (In bulk segregation) for Al concentrations higher than 10%. If the temperature were increased, we would observe two characteristics. First, the concentration of Al at which the phase separation occurs is shifted to a higher value, and second, the maximum value of the In-In affinity decreases. These two points can be explained by considering that, for high temperatures, the tendency towards phase separation is overcome by the thermal energy. Also, it is important to note that, even before the phase separation, there is a segregation of the ternary GaInN, as described in Sec. III B. A curious point in these results is that the increase in Al concentration favors In segregation, meaning that Al catalyzes the phase-separation process. In summary, this result shows how much this quaternary alloy is unstable. For the usual growth temperatures, and almost any composition in which the AlGaInN quaternary alloy is lattice matched to GaN, there is a tendency towards phase separation into In-rich regions.

Figures 11 and 12 present the study of the AlGaInP quaternary alloy lattice-matched to GaAs and the AlGaInAs quaternary alloy lattice-matched to InP. We chose the usual growth temperatures (973 K and 923 K for AlGaInP and AlGaInAs, respectively), and two or three other, smaller temperatures. As we can observe, the two epitaxial alloys are very stable. In the case of AlGaInP at 773 K some composition instabilities begin to appear. At 673 K and for low Al concentration, one notices a weak tendency to segregate in an In-rich phase and in an AlGaP ternary. The same occurs for AlGaInAs lattice-matched to InP, but only at 523 K. It is important to note that, for the two alloys, even at the low temperatures studied, there is no clear evidence for phase separation with 1 order of magnitude higher In-In affinity.

Experimentally it was observed that the arsenide and phosphide quaternary systems are very stable against phase separation in comparison with the nitrides. The AlGaInAs quaternary system can be easily grown by molecular beam epitaxy (MBE), with control over the whole range of alloy compositions, yielding high-quality materials. Experiments like Raman scattering by longitudinal optical phonons[33] show no evidence of features attributable to regions of dif-

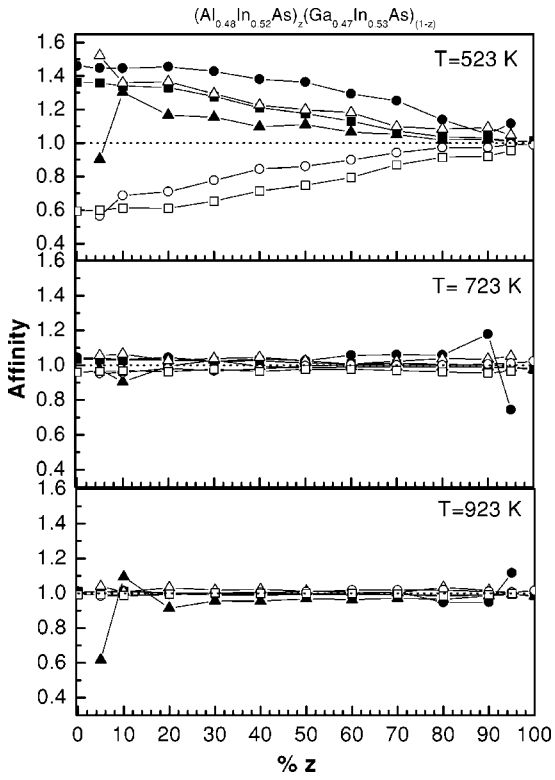

FIG. 12. Affinities versus *z* concentration in the region of composition where the AlGaInAs quaternary is lattice matched to InP. The affinities are represented by full triangles (Al-Al), full circles (Ga-Ga), full squares (In-In), empty triangles (Al-Ga), empty circles (Al-In), and empty squares (Ga-In).

ferent compositions and no clustering. For the phosphides ordering due to surface reconstructions was observed. This last aspect was not taken into account in our calculations, since we studied the existence of a miscibility gap without including surface effects. On the other hand, for all other aspects of thermodynamic stability, there is a very good agreement with our results.

IV. SUMMARY

Summarizing, we developed a different Monte Carlo approach for the study of quaternary alloys. We combined a modified ternary expansion method with MC simulations and *ab initio* DFT-LDA calculations. We applied our method tothe study of the III-V $Al_xGa_yIn_{1-x-y}N$, $Al_xGa_yIn_{1-x-y}P$, and $Al_xGa_yIn_{1-x-y}As$ quaternary alloys. We presented the results for the thermodynamic properties of these alloys, together with a microscopic description of the phase-separation process. A comparative study of the role of the different anions was made. Also, we made a complete microscopic description of AlGaInAs, AlGaInP, and AlGaInN with compositions that lattice-matched to InP, GaAs, and GaN substrates, respectively. We observed that the nitride alloys are prone to phase separation into In-rich phases, with the critical temperature close to the usual growth temperatures for the compositions commonly grown. For lower temperatures or for high In and/or Al concentrations, the alloy always presents phase separation. On the contrary, the arsenides and phosphides are very stable against phase separation, because the critical temperatures for segregation are far below their typical growth temperatures. In particular we observed a typical effect of composition fluctuations only in the nitride alloys, where inhomogeneities in the distribution of atoms take place towards the formation of GaInN and AlGaN ternary clusters.

ACKNOWLEDGMENT

This work was supported by the Brazilian funding agencies FAPESP and CNPq.

*Corresponding author. Electronic mail: scolfaro-@macbeth.if.usp.br

[1] G. B. Stringfellow, J. Appl. Phys. **54**, 404 (1983).
[2] D. Olego, T. Y. Chang, E. Silberg, E. A. Caridi, and A. Pinczuk, Appl. Phys. Lett. **41**, 476 (1982).
[3] T. Fujii, Y. Nakata, Y. Sigiyama, and S. Hiyiamizu, Jpn. J. Appl. Phys., Part 1 **25**, L254 (1986).
[4] D. J. Mowbray, O. P. Kowalski, M. Hopkinson, M. S. Skolnick, and J. P. R. David, Appl. Phys. Lett. **65**, 213 (1994).
[5] G. S. Chen, T. Y. Wang, and G. B. Stringfellow, Appl. Phys. Lett. **56**, 1463 (1990).
[6] P. Gavrilovic, F. P. Dabkowski, K. Meehan, J. E. Willians, W. Stutius, K. C. Hsieh, N. Holonyak, M. A. Shahid, and S. Mahajan, J. Cryst. Growth **93**, 426 (1988).
[7] T. Tanaka, H. Yanagisawa, H. Kakibayashi, S. Minagawa, and T. Kajimura, Appl. Phys. Lett. **59**, 1943 (1991).
[8] S. Nakamura, Semicond. Sci. Technol. **14**, R27 (1999).
[9] J. Li, K. B. Nam, K. H. Kim, J. Y. Lin, and H. X. Jiang, Appl. Phys. Lett. **78**, 61 (2001).
[10] M. Kneissl, D. W. Treat, M. Teepe, N. Miyashita, and N. M. Johnson, Appl. Phys. Lett. **82**, 2386 (2003).
[11] A. Yasan, R. McClintock, K. Mayes, S. R. Darvish, H. Zhang, P. Kung, M. Razeghi, S. K. Lee, and J. Y. Han, Appl. Phys. Lett. **81**, 2151 (2002).
[12] S. Nagahama, T. Yanamoto, M. Sano, and T. Mukai, Jpn. J. Appl. Phys., Part 1 **40**, L788 (2001).
[13] H. Hirayama, A. Kinoshita, T. Yamabi, Y. Enomoto, A. Hirata, T. Araki, Y. Nanishi, and Y. Aoyagi, Appl. Phys. Lett. **80**, 207

(2002).
[14] C. H. Chen, Y. F. Chen, Z. H. Lan, L. C. Chen, K. H. Chen, H. X. Jiang, and J. Y. Lin, Appl. Phys. Lett. **84**, 1480 (2004).
[15] S. W. Feng, Y. C. Cheng, Y. Y. Chung, C. C. Yang, K. J. Ma, C. C. Yan, C. Hsu, J. Y. Lin, and H. X. Jiang, Appl. Phys. Lett. **82**, 1377 (2003).
[16] L. G. Ferreira, S.-H. Wei, and A. Zunger, Int. J. Supercomput. Appl. **5**, 34 (1991).
[17] N. A. Zarkevich and D. D. Johnson, Phys. Rev. B **67**, 064104 (2003).
[18] R. Drautz, R. Singer, and M. Fähnle, Phys. Rev. B **67**, 035418 (2003).
[19] J. M. Sanchez, F. Ducastelle, and D. Gratias, Physica A **128**, 334 (1984).
[20] M. Marques, L. K. Teles, L.M. R. Scolfaro, J. R. Leite, J. Furthmuller, and F. Bechstedt, Appl. Phys. Lett. **83**, 890 (2003).
[21] G. Kresse and J. Furthmüller, Comput. Mater. Sci. **6**, 15 (1996); Phys. Rev. B **54**, 11169 (1996).
[22] N. Metropolis, A. W. Rosenbluth, M. N. Rosenbluth, A. H. Teller, and E. Teller, J. Chem. Phys. **21**, 1087 (1953).
[23] P. Hohenberg and W. Kohn, Phys. Rev. **136**, B864 (1965).
[24] D. Vanderbilt, Phys. Rev. B **41**, 7892 (1990).
[25] J. P. Perdew and A. Zunger, Phys. Rev. B **23**, 5048 (1981).
[26] H. J. Monkhorst and J. D. Pack, Phys. Rev. B **13**, 5188 (1974).
[27] L. Vegard, Z. Phys. **5**, 17 (1921).
[28] J. M. Cowley, J. Appl. Phys. **21**, 24 (1950).
[29] S. -H. Wei, L. G. Ferreira, J. E. Bernard, and A. Zunger, Phys. Rev. B **42**, 9622 (1990).
[30] L. K. Teles, J. Furthmüller, L. M. R. Scolfaro, J. R. Leite, and F. Bechstedt, Phys. Rev. B **62**, 2475 (2000).
[31] L. K. Teles, L. M. R. Scolfaro, J. R. Leite, J. Furthmller, and F. Bechstedt, J. Appl. Phys. **92**, 7109 (2002).
[32] M. Marques, L. K. Teles, L. M. R. Scolfaro, L. G. Ferreira, and J. R. Leite, Phys. Rev. B **70**, 073202 (2004).
[33] R. Borroff, R. Merlin, A. Chin, and P. K. Bhattacharya, Appl. Phys. Lett. **53**, 1652 (1988).
[34] V. Ozoliņš, C. Wolverton, and A. Zunger, Phys. Rev. B **57**, 6427 (1998).